Available online at www.sciencedirect.com
SCIENCE DIRECT®
Journal of Solid State Chemistry 177 (2004) 257–261
JOURNAL OF SOLID STATE CHEMISTRY
http://elsevier.com/locate/jssc

Syntheses and characterization of the actinide manganese selenides $ThMnSe_3$ and $UMnSe_3$

Ismail Ijjaali, Kwasi Mitchell, Fu Qiang Huang, and James A. Ibers*

Department of Chemistry, Northwestern University, 2145 Sheridan Road, Evanston, IL 60208-3113, USA

Received 29 May 2003; received in revised form 24 July 2003; accepted 1 August 2003

Abstract

The $An MnSe_3$ (An = Th, U) compounds were synthesized from high-temperature solid-state reactions of the constituent elements at 1223 and 1273 K, respectively. Both compounds are isostructural with $UFeS_3$ and crystallize in the space group *Cmcm* of the orthorhombic system with four formula units in a cell. Cell constants (Å) at 153 K are: $ThMnSe_3$, 4.0304(4), 12.795(1), 9.2883(9); $UMnSe_3$, 3.931(5), 12.705(14), 9.148(10). The structure comprises layers of $MnSe_6$ octahedra that alternate with layers of $AnSe_8$ bicapped trigonal prisms along the *b*-axis. Because there are no Se–Se bonds in the structure of $An MnSe_3$ the formal oxidation states of An/Mn/Se are $4+/2+/2-$. $UMnSe_3$ is a ferromagnet with $T_C = 62$ K.

Keywords: Synthesis; Crystal structure; Solid-state compound; Uranium manganese selenide; Thorium manganese selenide; Ferromagnet

1. Introduction

A number of $An/M/Q$ phases (An = Th or U); M = 3*d*-transition metal; Q = S or Se or Te) have been isolated [1]. However, single-crystal X-ray diffraction studies have only been conducted on a few of these phases. These include the U phases $UFeS_3$ [2], $UCrS_3$ [3], U_2FeS_5 [4], $U_2Cu_{0.78}Te_6$ [5], $U_2Cu_xTe_6$ ($x = 0.25$, 0.33) [6], $U_3Cu_2Q_7$ (Q = S, Se) [7], $U_6Cu_2Q_{13}$ (Q = S, Se) [8,9], U_8FeS_{17} [10], and U_8CrS_{17} [11] and the Th phases $ThMTe_3$ (M = Mn, Mg) [12] and Th_2CuTe_6 [13]. Although these ternary actinide chalcogenides were initially investigated over four decades ago, a detailed understanding of the relationship between the magnetic and structural properties of these materials has yet to evolve. Owing to the complex magnetic behavior of the 5*f* electrons of the actinides, a thorough investigation of the structural properties of the $An/M/Q$ phases is necessary to draw correlations between the structural and magnetic properties of the materials. In this paper, we report the first single-crystal study of the Mn/Se representatives of $An MnSe_3$ phase, $UMnSe_3$ and $ThMnSe_3$, in addition to the magnetic properties of $UMnSe_3$.

2. Experimental

2.1. Syntheses

Th and U metal were handled in an argon-filled glovebox to prevent exposure to oxygen and moisture. Crystals of $ThMnSe_3$ were synthesized from the direct combination of the elements at 1223 K. Stoichiometric amounts of Th (111 mg, Johnson Matthey, 99.8%), Mn (26 mg, Alfa Aesar, 99.9%), and Se (113 mg, Alfa Aesar, 99.5%) were mixed and sealed in a fused-silica tube that was then evacuated to $\sim 10^{-4}$ Torr. About 180 mg of Sn was added to promote crystal growth. The sample was then placed in horizontal tube furnace, reacted at 1223 K for 6 days, and cooled at 3°C/hour. Crystals, which grew as black blocks with dimensions on the order of 0.07 mm, were manually extracted from the reaction mixture. This reaction produces only a few crystals of $ThMnSe_3$. Most of the products were amorphous unreacted material and spherical droplets of elemental Sn.

Black needles of $UMnSe_3$ formed from the reaction of U (119 mg, Omega Chemicals, 99.8%), Mn (27 mg), and Se (120 mg) in a KBr flux (~350 mg, Alfa Aesar, 99%). The materials were mixed and sealed in a fused-silica tube that was then evacuated to $\sim 10^{-4}$ Torr. The tube was heated to 1273 K in 60 h, kept at 1273 K for 50 h,

*Corresponding author. Fax: +1-847-491-2976.
E-mail address: ibers@chem.northwestern.edu (J.A. Ibers).

0022-4596/$ - see front matter © 2003 Elsevier Inc. All rights reserved.
doi:10.1016/j.jssc.2003.08.004

cooled at 4 K/h to 473 K, and then the furnace was turned off. The reaction mixture was washed free of bromide salts with water and then dried with acetone. The yield of the reaction was approximately 50% (based upon U).

Selected single crystals of each compound were examined with an EDX-equipped Hitachi 3500N SEM and found to have the stated composition within the accuracy of the method ($\pm 5\%$). Both compounds are stable in air.

2.2. Crystallography

For each compound a single crystal was mounted directly in the cold stream (153 K) of a Bruker Smart-1000 CCD diffractometer [14]. Graphite-monochromatized Mo$K\alpha$ radiation ($\lambda = 0.71073$ Å) was used. The crystal-to-detector distance was 5.023 cm. Data were collected by a scan of 0.3° in ω in groups of 606, 606, 606, and 606 frames at ϕ settings of 0°, 90°, 180°, and 270°. The exposure time was 15 s/frame. The collection of intensity data on the Bruker diffractometer was carried out with the program SMART [14]. Cell refinement and data reduction were carried out with the use of the program SAINT [14] and a face-indexed absorption correction was performed numerically with the use of the program XPREP [15]. The program SADABS [14] was then employed to make incident beam and decay corrections.

The structures were solved with the direct methods program SHELXS and refined with the full-matrix least-squares program SHELXL of the SHELXTL suite of programs [15]. Each final refinement included anisotropic displacement parameters and a secondary extinction correction. The program STRUCTURE TIDY [16] was used to standardize the positional parameters. Additional crystallographic details are given in Table 1. Fractional coordinates and equivalent atomic displacement parameters are listed in Table 2. Table 3 presents selected interatomic distances.

2.3. Magnetic susceptibility

Measurements on single crystals of $UMnSe_3$ (4.4 mg) were carried out with the use of a Quantum Design SQUID magnetometer (MPMS5 Quantum Design). The composition of the sample was verified by EDX measurements. The sample was loaded into a gelatin capsule and magnetic susceptibility measurements were collected between 5 and 300 K by means of a zero-field cooling–field cooling (ZFC–FC) procedure with an applied field of 20 kG. Data were corrected for the diamagnetic contributions of the atomic cores [17].

Table 1
Crystal data and experimental details for $An MnSe_3$

Formula	$ThMnSe_3$	$UMnSe_3$
Formula weight	523.86	529.85
Space group	*Cmcm*	*Cmcm*
a (Å)	4.0304(4)	3.931(5)
b (Å)	12.795(1)	12.705(14)
c (Å)	9.2883(9)	9.148(10)
V (Å^3)	478.99(8)	456.9(9)
Z	4	4
T (K)	153	153
ρ_c (g/cm^3)	7.264	7.702
Linear abs. coeff. (cm^{-1})	562.44	618.48
Transm. factors	0.075–0.178	0.014–0.189
$R(F)$[a] ($F_o^2 > 2\sigma(F_o^2)$)	0.0183	0.0239
$R_w(F_o^2)$[b] (all data)	0.0449	0.0604

[a] $R(F) = \sum \| F_o | - | F_c \| / \sum | F_o |$.

[b] $R_w(F_o^2) = [\sum w(F_o^2 - F_c^2)^2 / \sum w F_o^4]^{1/2}$, $w^{-1} = \sigma^2(F_o^2) + (q \times F_o^2)^2$ for $F_o^2 > 0$; $w^{-1} = \sum^2(F_o^2)$ for $F_o^2 \leqslant 0$. $q = 0.02$ for $ThMnSe_3$ and 0.03 for $UMnSe_3$.

Table 2
Atomic coordinates and equivalent isotropic displacement parameters for $An MnSe_3$

Atom	x	y	z	U_{eq} (A^2)[a]
$ThMnSe_3$				
Th	0	0.74907(2)	1/4	0.0026(2)
Mn	0	0	0	0.0066(3)
Se(1)	0	0.35502(5)	0.05864(7)	0.0033(2)
Se(2)	0	0.08274(7)	1/4	0.0032(2)
$UMnSe_3$				
U	0	0.74949(3)	1/4	0.0100(2)
Mn	0	0	0	0.0170(4)
Se(1)	0	0.35334(6)	0.06038(8)	0.0105(3)
Se(2)	0	0.08702(8)	1/4	0.0105(3)

[a] U_{eq} is defined as one-third of the trace of the orthogonalized U_{ij} tensor.

Table 3
Selected distances (Å) for $An MnSe_3$

	$ThMnSe_3$	$UMnSe_3$
An–Se(2) × 2	2.9309(7)	2.850(2)
An–Se(1) × 4	3.0096(5)	2.935(2)
An–Se(1) × 2	3.1611(7)	3.126(3)
$An \cdots$ Mn	3.9623(4)	3.919(1)
Mn–Se(2) × 2	2.5520(4)	2.540(2)
Mn–Se(1) × 4	2.7926(5)	2.764(2)

3. Results and discussion

$ThMnSe_3$ and $UMnSe_3$ are isostructural with $UFeS_3$ [2]. A view of the unit cell is depicted in Fig. 1. It consists of a three-dimensional framework in which layers of $MnSe_6$ octahedra alternate with layers of $AnSe_8$ bicapped trigonal prisms along the b-axis. As shown in

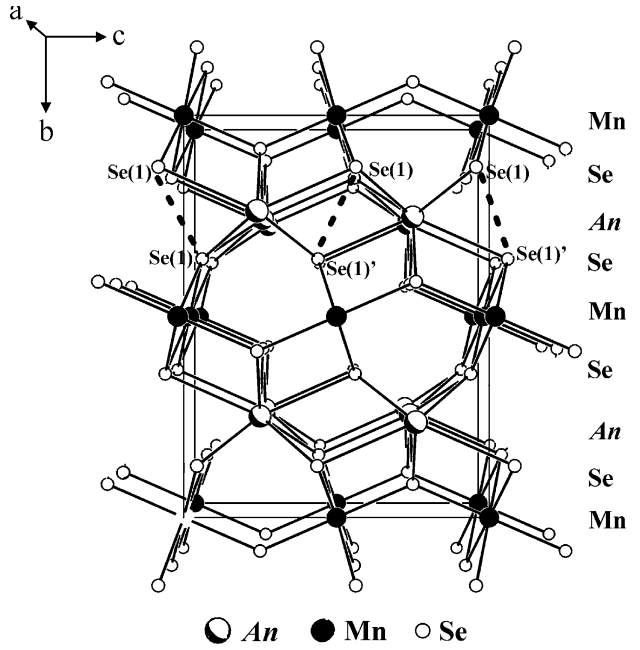

Fig. 1. Unit cell of AnMnSe$_3$ (An = Th, U) viewed down the a-axis.

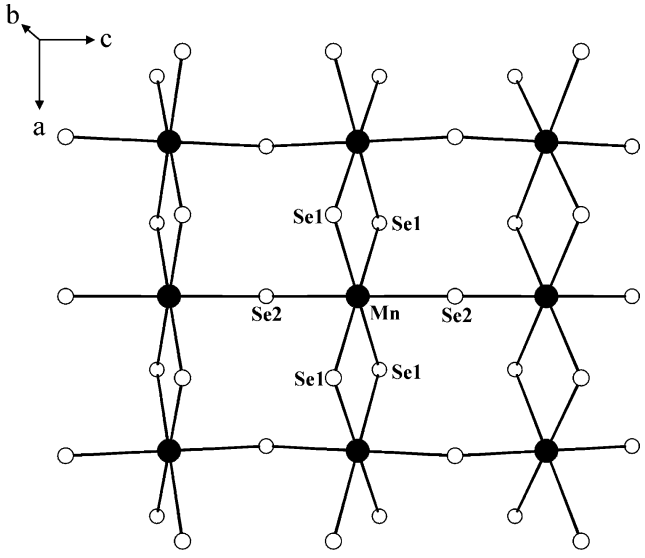

Fig. 2. MnSe$_6$ layer viewed down the a-axis.

Fig. 2, the MnSe$_6$ octahedra share Se(1)–Se(1) edges along the a-axis and Se(2) corners along the c-axis to form an infinite buckled sheet. The AnSe$_8$ bicapped trigonal prisms (Fig. 3) share edges and caps to form a spacer layer that separates the sheets of MnSe$_6$ octahedra. The AnSe$_8$ and MnSe$_6$ polyhedra participate in edge- and corner-sharing to bind the layers together and form the overall three-dimensional structure.

The infinite buckled sheet of transition-metal centered octahedra found in the present AnMnSe$_3$ compounds is also encountered in the UCrS$_3$ distorted perovskite structure ($GdFeO_3$ structure type) [3]. A number of

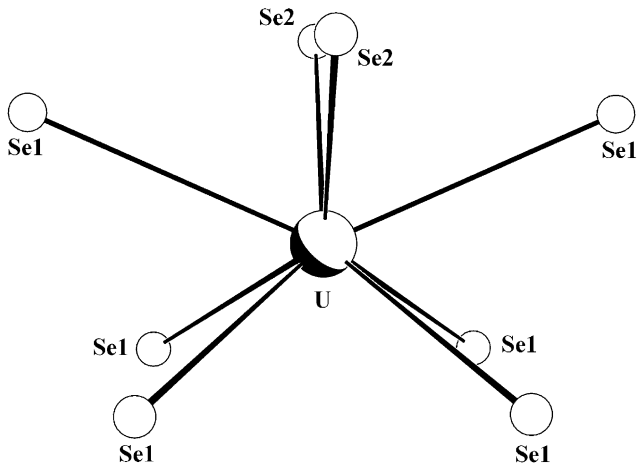

Fig. 3. Coordination environment of An in AnMnSe$_3$.

actinide-metal transition-metal chalcogenides adopt the UCrS$_3$ structure and crystallize in the space group $Pnma$ of the orthorhombic system, including UMS$_3$ (M = V, Cr, Co, Ni, Ru, Rh) and UMSe$_3$ (M = V, Cr, Co, Ni), whereas only UFeSe$_3$, ThMnTe$_3$, and the present compounds adopt the UFeS$_3$ structure type [1,12]. The UCrS$_3$ structure is related to that of the AnMnSe$_3$ compounds and is composed of layers of corner-sharing CrS$_6$ octahedra. However, in UCrS$_3$ the CrS$_6$ layers are condensed and the octahedra participate in additional corner-sharing along the b-axis to form a three-dimensional tunnel network in which the U atoms reside (Fig. 4). Conversely, one may also imagine that the structure of the AnMnSe$_3$ compounds may be compressed so that the MnSe$_6$ layers connect via the Se1 or Se1′ atoms (Fig. 1). This modification would form the tunnel network evident in the UCrS$_3$ structure. The reason for the formation of the layered UFeS$_3$ structure as opposed to the UCrS$_3$ tunnel structure is unknown.

Ordered phases with the Mn^{2+} cation octahedrally coordinated by Se atoms are uncommon. Examples we can find are MnSe, which adopts the rock salt [18] and NiAs [19] structures, and Mn_2SiSe_4, which crystallizes in the olivine structure type [20]. The Mn–Se distances, which range from 2.540(2) to 2.7926(5) Å in the present compounds (Table 3), are consistent with those of 2.685(2)–2.756(3) Å in Mn_2SiSe_4 [20]. Other distances in the present compounds are also normal. Thus the An–Se distances, which range from 2.850(2) to 3.1611(7) Å, are consistent, for example, with those of 2.962(1)–3.0153(6) Å for Th–Se in KTh_2Se_6 [21] and 2.868(2)–3.041(1) Å for U–Se in UPdSe$_3$ [22]. Because there are no Se–Se bonds in the structure of AnMnSe$_3$ the formal oxidation states of An/Mn/Se are 4+/2+/2−.

A plot of the molar susceptibility (χ) vs. T for UMnSe$_3$ is shown in Fig. 5. The compound exhibits a ferromagnetic transition at approximately 62 K. The

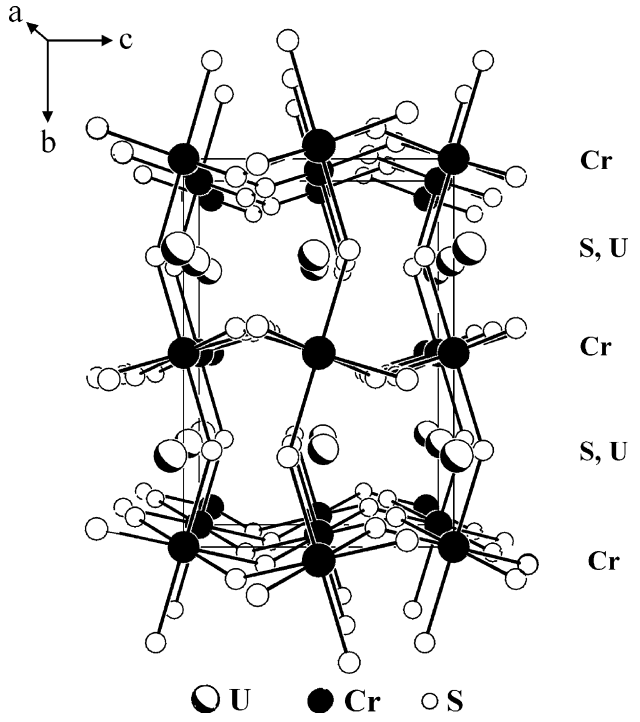

Fig. 4. Unit cell of $UCrS_3$ viewed down the *a*-axis. The U–S bonds have been removed for clarity.

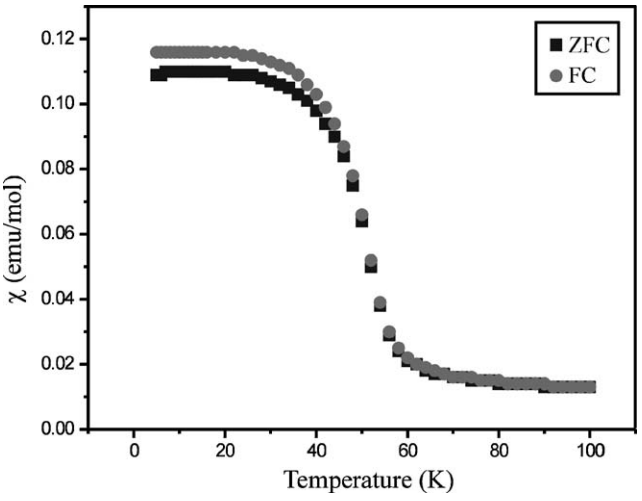

Fig. 5. Zero-field cooled (ZFC) and field cooled (FC) magnetic susceptibility data (χ) vs. T for $UMnSe_3$.

slight differences observed between the ZFC–FC susceptibility data below 50 K arise from magnetocrystalline anisotropy. This effect disappears when a sufficiently high field is applied or a high enough temperature is reached. Similar deviations were detected for the $U_3Z_xTe_5$ (Z = Ge, Sn) ferromagnets [23]. The high-temperature susceptibility data ($T > 200$ K) were fit by a least-squares method to the Curie–Weiss equation $\chi = C/(T-\theta_p)$, where C is the Curie constant and θ_p is the Weiss constant. The effective magnetic moment (μ_{eff}) was calculated from the equation $\mu_{eff} = (7.997C)^{1/2}\,\mu_B$ [24]. The values obtained are $C = 4.60(2)$ emu K mol^{-1}, $\theta_p = 50.0(2)$ K, and $\mu_{eff} = 6.06(4)\,\mu_B$. As is typical of U chalcogenides, μ_{eff} is lower than the theoretical value of $6.92\,\mu_B$, calculated from the theoretical magnetic moments for U^{4+} and Mn^{2+} of 3.58 and $5.92\,\mu_B$, respectively. This may be attributed to crystal field effects or to 5*f* electron delocalization or both. Similar effects are observed in the magnetic properties of U_2Te_3 [25], U_3Te_5 [26], $U_3Z_xTe_5$ (Z = Ge, Sn) [23], U_7Te_{12} [27], $UCoS_3$ [28], $URuS_3$ [29], and $U_{0.82}Mo_6Se_8$ [30].

Acknowledgments

This research was supported by the US National Science Foundation under Grant DMR00-96676 (J.A.I.) and a Ford Predoctoral Fellowship to K.M. Use was made of the Central Facilities supported by the MRSEC program of the National Science Foundation (DMR00-76097) at the Materials Research Center of Northwestern University.

References

[1] A.A. Narducci, J.A. Ibers, Chem. Mater. 10 (1998) 2811–2823.
[2] H. Noël, J. Padiou, Acta Crystallogr. Sect. B: Struct. Crystallogr. Cryst. Chem. 32 (1976) 1593–1595.
[3] H. Noël, J. Padiou, J. Prigent, C. R. Seances Acad. Sci. Ser. C 280 (1975) 123–126.
[4] H. Noël, M. Potel, J. Padiou, Acta Crystallogr. Sect. B: Struct. Crystallogr. Cryst. Chem. 32 (1976) 605–606.
[5] F.Q. Huang, J.A. Ibers, J. Solid State Chem. 159 (2001) 186–190.
[6] R. Patschke, J.D. Breshears, P. Brazis, C.R. Kannewurf, S.J.L. Billinge, M.G. Kanatzidis, J. Am. Chem. Soc. 123 (2001) 4755–4762.
[7] A. Daoudi, M. Lamire, J.C. Levet, H. Noël, J. Solid State Chem. 123 (1996) 331–336.
[8] H. Noël, M. Potel, J. Less-Common Metals 113 (1985) 11–15.
[9] H. Noël, J. Less-Common Metals 72 (1980) 45–49.
[10] H. Kohlmann, K. Stöwe, H.P. Beck, Z. Anorg. Allg. Chem. 623 (1997) 897–900.
[11] H. Noël, M. Potel, J. Padiou, Acta Crystallogr. Sect. B: Struct. Crystallogr. Cryst. Chem. 31 (1975) 2634–2637.
[12] A.A. Narducci, J.A. Ibers, Inorg. Chem. 39 (2000) 688–691.
[13] A.A. Narducci, J.A. Ibers, Inorg. Chem. 37 (1998) 3798–3801.
[14] Bruker, SMART Version 5.054 Data Collection and SAINT-Plus Version 6.22 Data Processing Software for the SMART System, 2000 (Bruker Analytical X-ray Instruments, Inc., Madison, WI, USA).
[15] G.M. Sheldrick, SHELXTL DOS/Windows/NT Version 6.12, 2000 (Bruker Analytical X-ray Instruments, Inc., Madison, WI, USA).
[16] L.M. Gelato, E. Parthé, J. Appl. Crystallogr. 20 (1987) 139–143.
[17] L.N. Mulay, E.A. Boudreaux, Theory and Applications of Molecular Diamagnetism, Wiley-Interscience, New York, 1976.
[18] A. Baroni, Z. Kristallogr, Kristallgeom. Kristallphys. Kristallchem. 99 (1938) 336–339.

[19] L. Cemic, A. Neuhaus, High Temp.-High Pressures 4 (1972) 97–99.
[20] S. Jobic, F. Bodénan, P. Le Boterf, G. Ouvrard, J. Alloys Compd. 230 (1995) 16–22.
[21] K.-S. Choi, R. Patschke, S.J.L. Billinge, M.J. Waner, M. Dantus, M.G. Kanatzidis, J. Am. Chem. Soc. 120 (1998) 10706–10714.
[22] A. Daoudi, H. Noël, J. Less-Common Metals 153 (1989) 293–298.
[23] O. Tougait, M. Potel, H. Noël, J. Solid State Chem. 168 (2002) 217–223.
[24] C.J. O'Connor, Prog. Inorg. Chem. 29 (1982) 203–283.
[25] O. Tougait, M. Potel, J.C. Levet, H. Noël, Eur. J. Solid State Inorg. Chem. 35 (1998) 67–76.
[26] O. Tougait, M. Potel, H. Noël, J. Solid State Chem. 139 (1998) 356–361.
[27] O. Tougait, M. Potel, H. Noël, Inorg. Chem. 37 (1998) 5088–5091.
[28] B. Chenevier, P. Wolfers, M. Bacmann, H. Noël, C. R. Acad. Sci., Sér. 2 (293) (1981) 649–652.
[29] A. Daoudi, H. Noël, Inorg. Chim. Acta 140 (1987) 93–95.
[30] A. Daoudi, M. Potel, H. Noël, J. Alloys Compd. 232 (1996) 180–185.